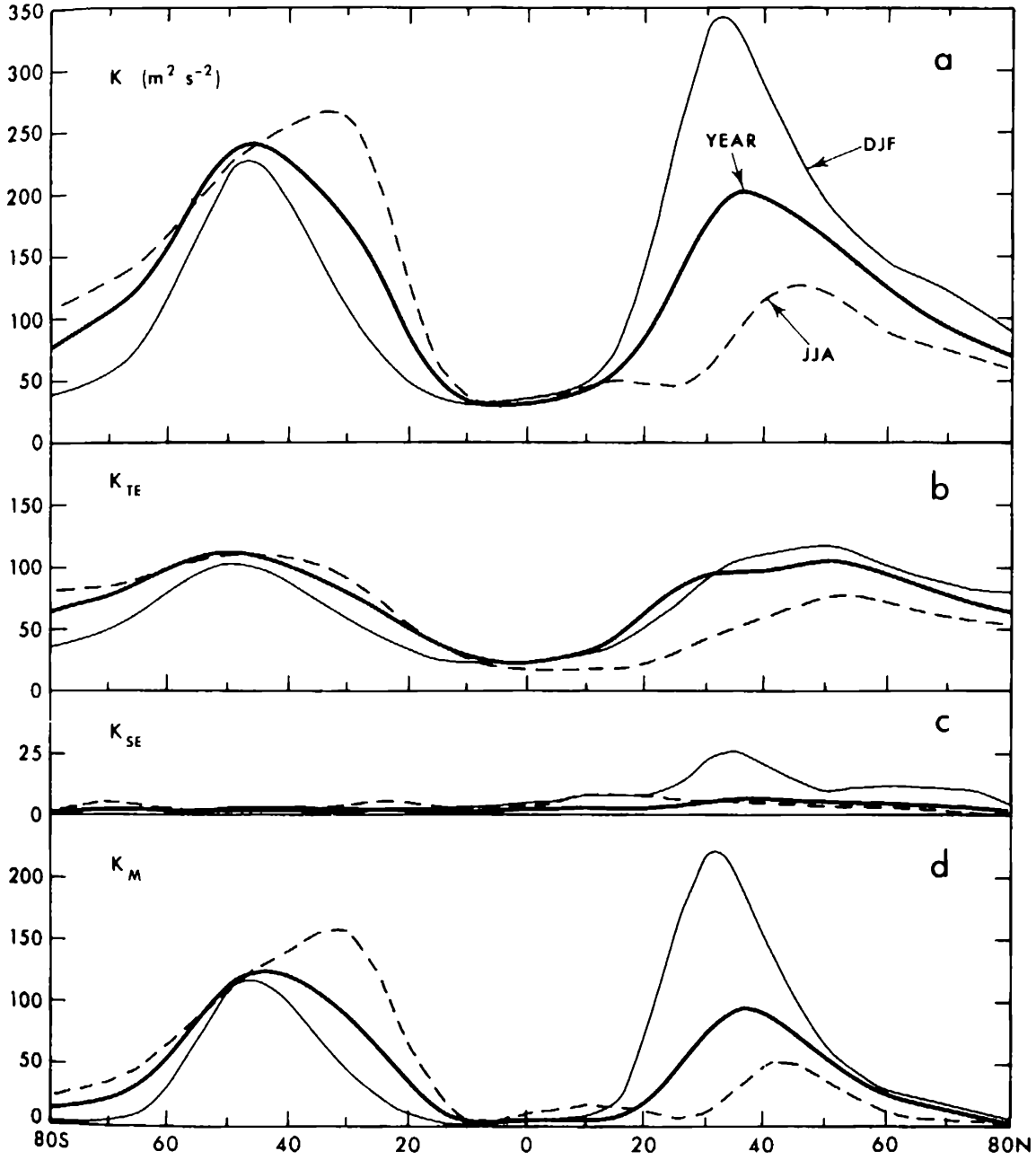

FIGURE 7.23. Meridional profiles of the zonal- and vertical-mean values of the total kinetic energy (a) and the transient eddy (b), stationary eddy (c), and mean meridional (d) components of the kinetic energy in $m^2 s^{-2}$ for annual, DJF, and JJA mean conditions (from Oort and Peixoto, 1983).

7.6 PRECIPITATION, EVAPORATION, RUNOFF, AND CLOUDINESS

7.6.1 Precipitation

Precipitation is one of the principal climatic elements. It is highly variable in space and time. Nevertheless, its average values are fairly stable and can be represented well in map form. So we will start with a discussion of Fig. 7.24 which shows

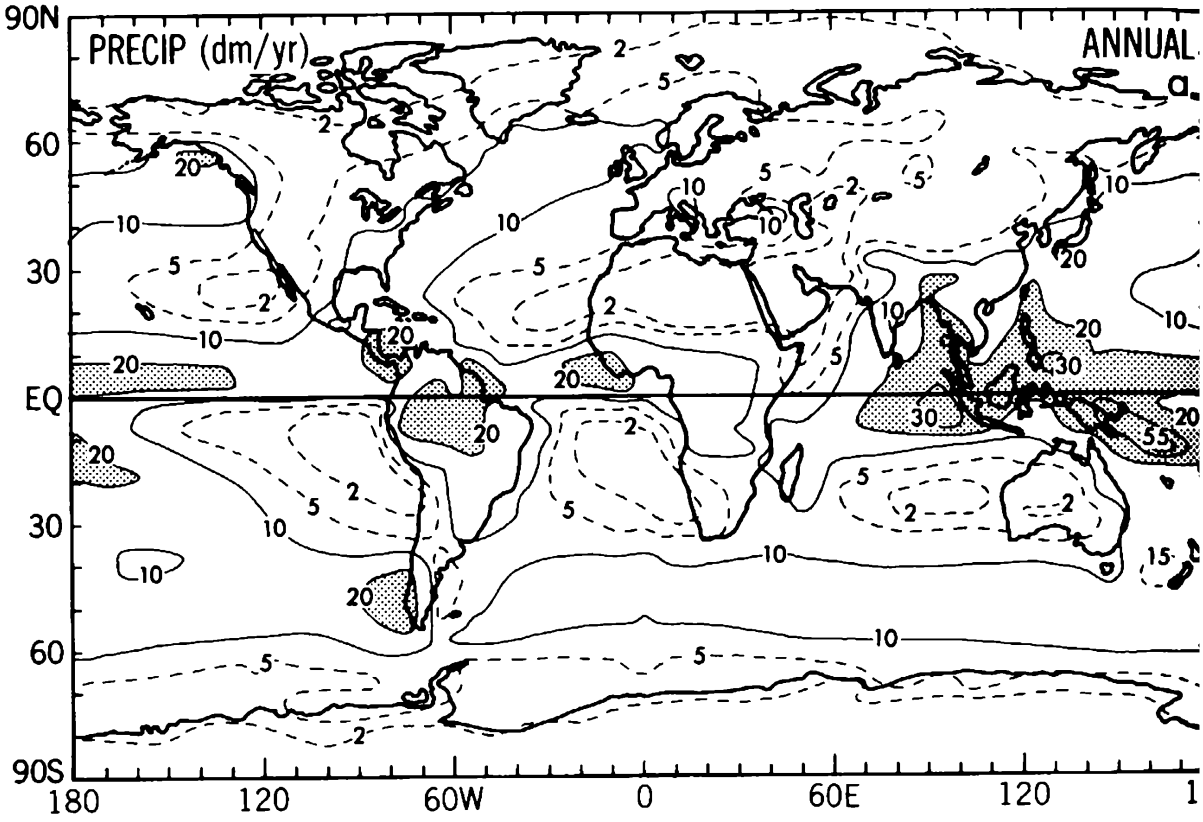

FIGURE 7.24a

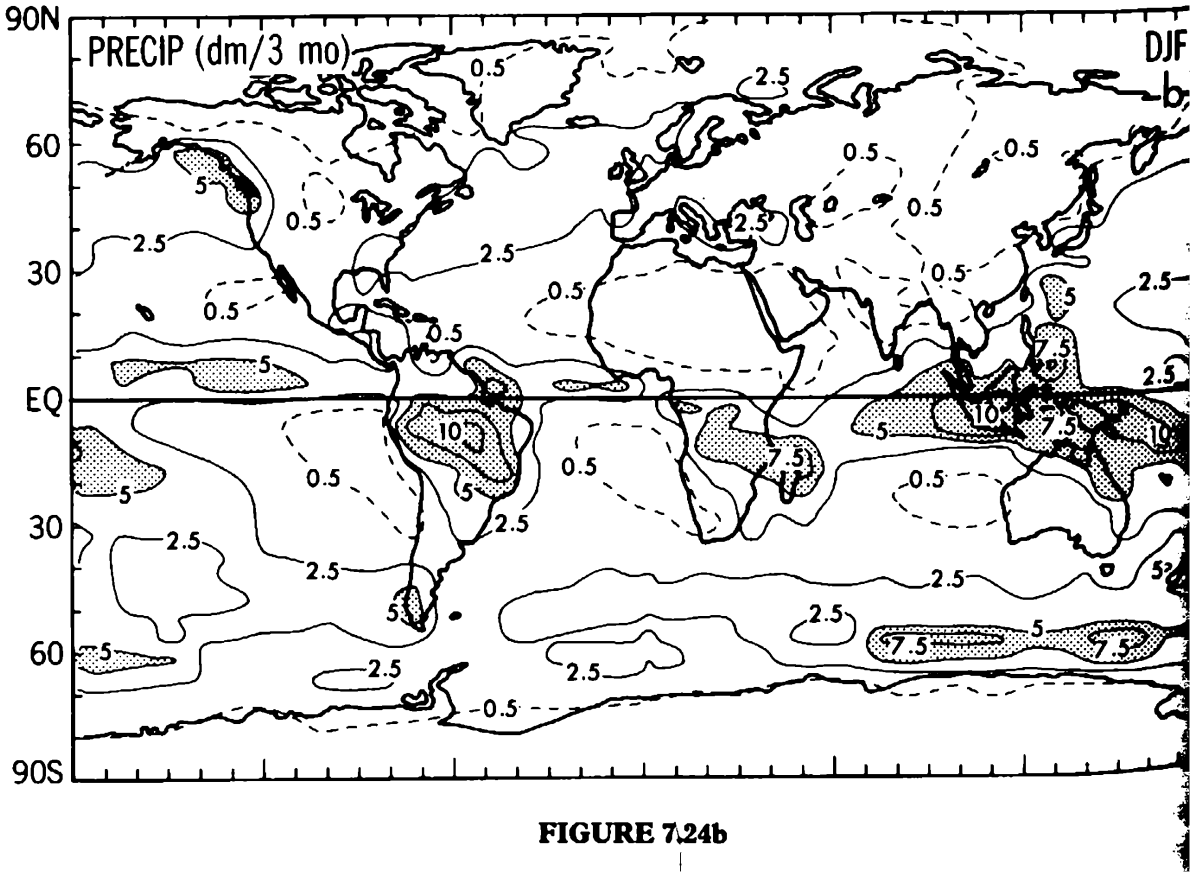

FIGURE 7.24b

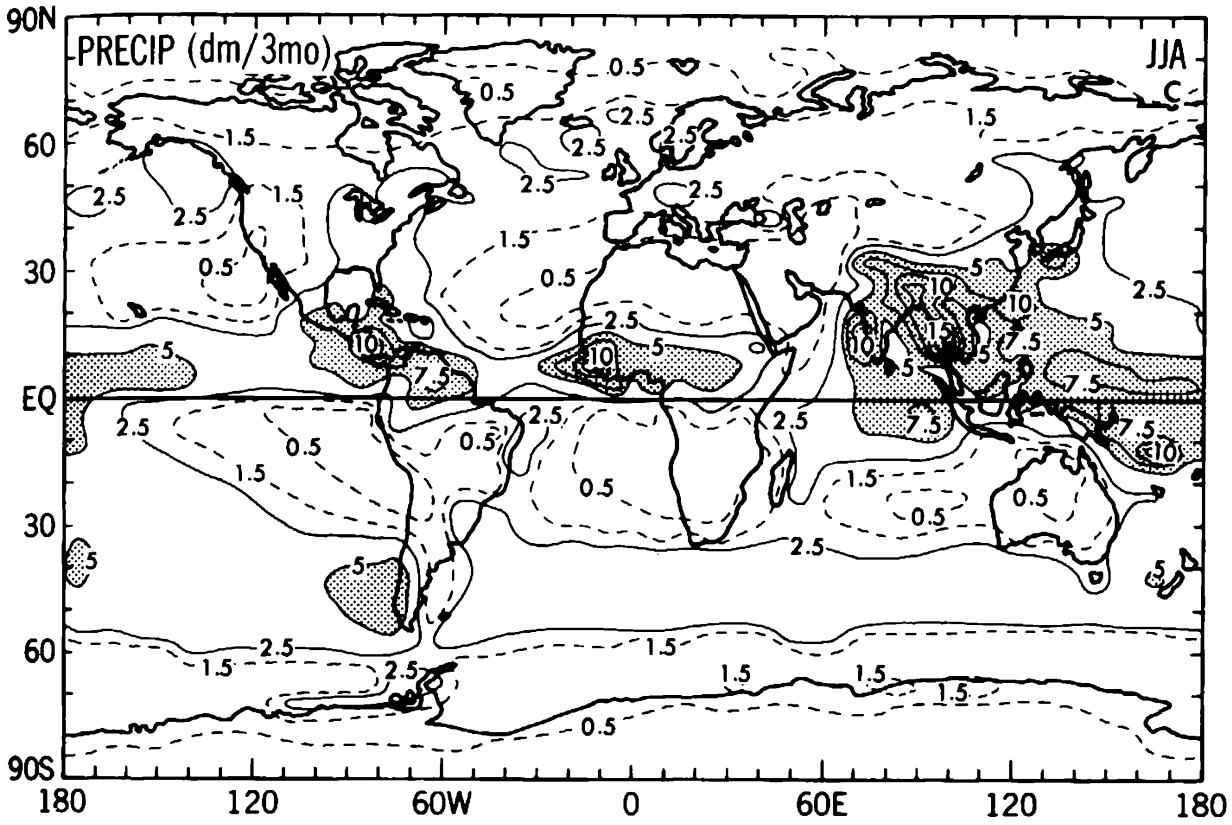

FIGURE 7.24. Global distributions of the precipitation rate for annual-mean conditions (a) in dm yr^{-1}, and for DJF (b) and JJA (c) conditions in dm (3 months) $^{-1}$, based on data from Jaeger (1976). Note that a precipitation rate of 1 m yr^{-1} corresponds to a release of latent heat in the atmosphere of about 79 W m^{-2}.

the distribution of precipitation according to Jaeger (1976) based on the surface station network [see Fig. 5.1(b)]. Note that the units on the maps are dm yr^{-1} for the annual mean and dm (3 months) $^{-1}$ for the seasons. The annual and seasonal distributions clearly reveal the influence of the oceans and continents. We should also mention that the precipitation data are very uncertain over the oceans because of the difficulties in directly measuring precipitation from ships.

The most significant features of the distribution are the high rainfall in equatorial latitudes associated with the strong convection in the ITCZ. Especially noteworthy are the very high values of precipitation over the equatorial regions in South America, Africa, and Indonesia and in the equatorial Pacific Ocean where precipitation may exceed 3 m yr^{-1} During the course of the year the ITCZ migrates north and south in phase with the solar insolation which explains the shift of the maxima in Figs. 7.24(b) and 7.24(c). There is a striking contrast in the seasonal maps over southeast Asia, which is mainly due to the Indian southwest monsoon dominating the summer circulation over the Horn of Africa, India, and southeast Asia.

Subsidence and low precipitation rates often less than 0.2 m yr^{-} dominate in many of the subtropical regions which are under the influence of the large semipermanent anticyclones. Large parts of the subtropical continents, such as in Africa and Australia, are covered by deserts, where the precipitation is very low. During the annual cycle the high-pressure centers migrate north and south causing summer dryness or semi-arid conditions in each hemisphere at the poleward side and winter dryness at the equatorial side of their annual-mean positions.

There is a secondary maximum in precipitation over midlatitudes where the polar fronts and the associated disturbances predominate. Here, precipitation is abundant during all seasons, except on their equatorial border where dryness prevails during the summer season when the high-pressure anticyclones move poleward, such as in the Mediterranean region.

Over the polar regions the moisture content of the atmosphere is very low, and the amounts of precipitation are less than 0.2 m yr^{-1} during all seasons.

The land–sea contrasts as well as seasonal differences become even clearer when we compare the zonal-mean profiles in Fig. 7.25. The seasonal shifts of the ITCZ are found to be more pronounced over land than over the oceans. The seasonal migration of the ITCZ is the determining factor in the existence of the marginal climates bordering the arid subtropical regions, such as are found in the Sahel belt in Africa.

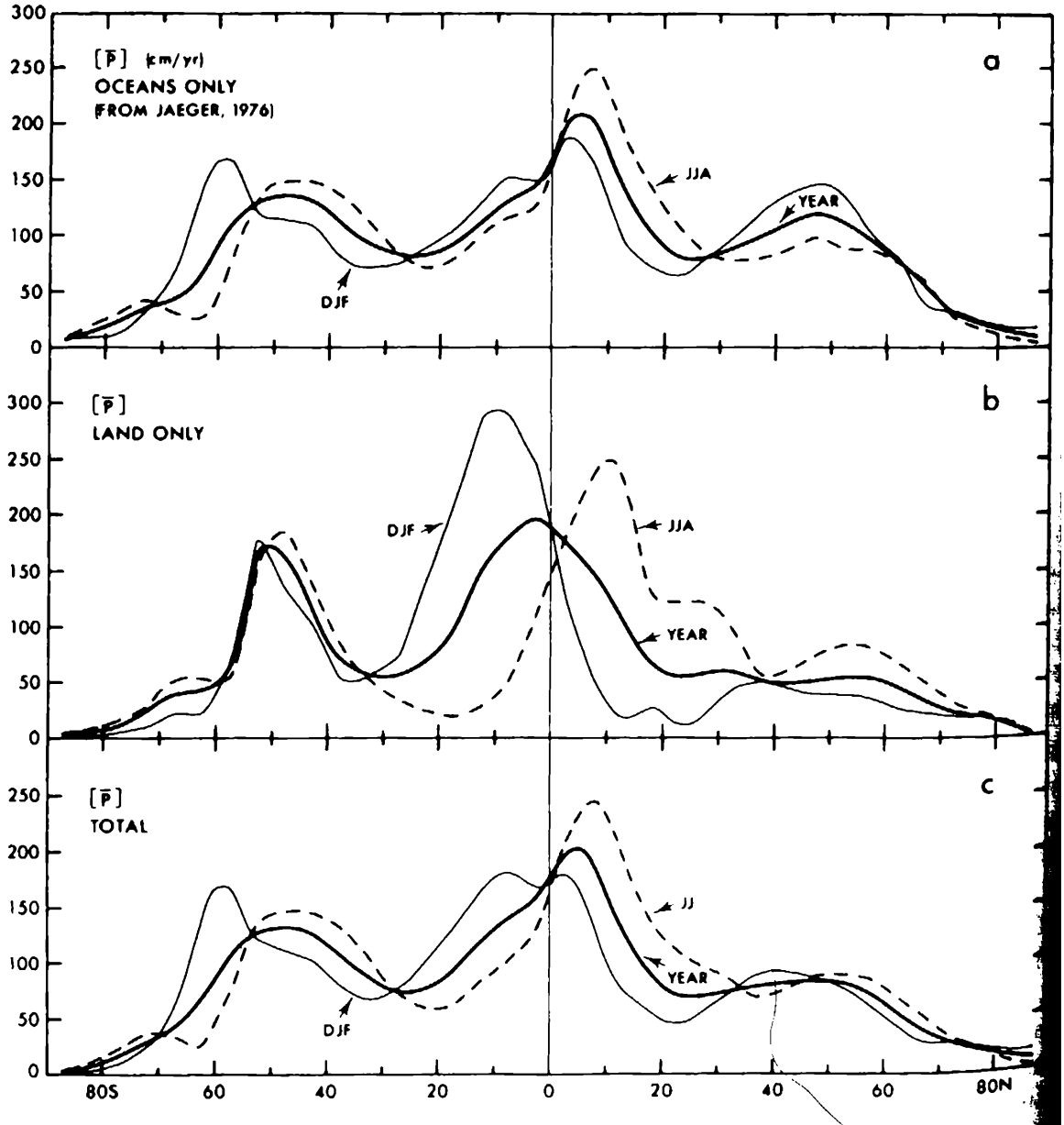

FIGURE 7.25. Meridional profiles of the zonal-mean precipitation rate in cm yr^{-1} for the ocean area (a), the land area (b), and the total land plus ocean area (c) for annual, DJF, and JJA mean conditions based on data from Jaeger (1976).

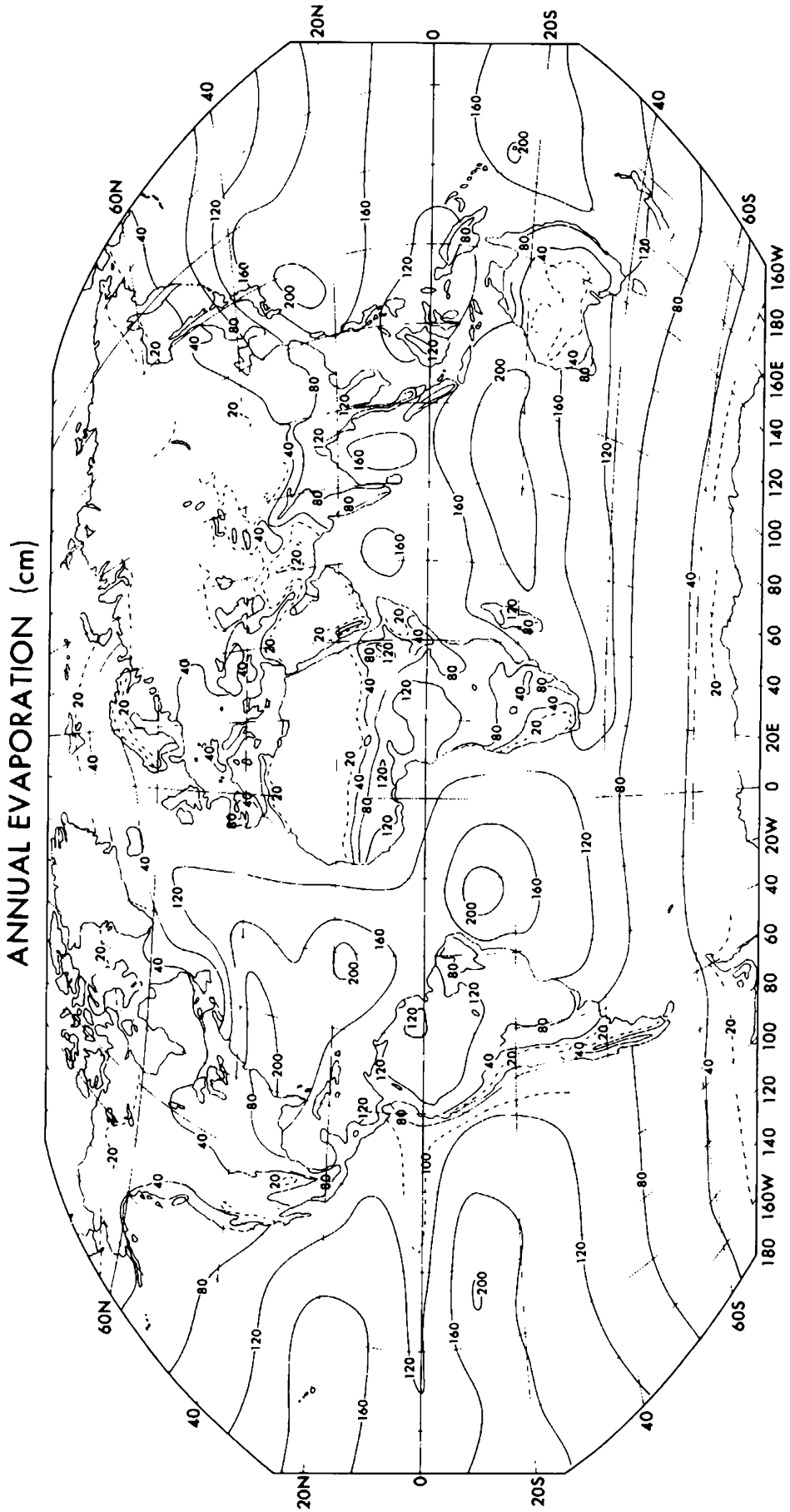

FIGURE 7.26. Global distribution of the annual-mean evaporation rate in cm yr^{-1} after Baumgartner and Reichel (1975).

7.6.2 Evaporation

The evaporation rate depends on many factors. The most important ones are the incoming radiation, temperature, wind speed, humidity, stability of the air, and the availability of water. Evaporation is often measured with a shallow circular pan. However, such measurements are much influenced by local conditions and local exposure. Thus, useful as they may be for local purposes, such as assessing evaporation from water reservoirs, small lakes, and irrigated areas, they are of little use in computing the water budget over larger regions of the earth.

Using surface ship data the evaporation over the oceans can also be evaluated from an approximate, empirically derived expression:

$$\overline{E} = -\rho C_w \overline{|V|(q_a - q_s)},$$

where ρ is the density of air, C_w the coefficient of eddy diffusion (≈ 0.0013), q_s the saturated specific humidity at the sea surface temperature, and q_a the specific humidity at a standard height of about 10 m above the surface. The foundations of this method will be discussed in Chap. 10.

Figure 7.26 shows the annual-mean evaporation as estimated by Baumgartner and Reichel (1975) using a variety of methods. The map shows that the highest values of evaporation occur over the subtropical oceans, where the oceanic "deserts" are found. The effects of warm and cold ocean currents and land–sea differences are very important, as illustrated by the midlatitude (mainly winter) maxima in evaporation, on the order of 2 m yr^{-1}, over the relatively warm Gulf Stream and Kuroshio currents to the east of the two major continents. Over the equatorial oceans, where precipitation is abundant, evaporation is less intense due to weaker winds and relatively low sea surface temperatures in the oceanic upwelling regions. Over the continents maximum evaporation occurs in the equatorial belt, mainly due to the higher precipitation and higher temperatures observed there.

Annual and seasonal profiles of the zonal-mean oceanic evaporation based on the bulk aerodynamic method are shown in Fig. 7.27 together with Baumgartner and Reichel's (1975) annual-mean estimates. The differences reflect the considerable uncertainties involved in estimating the evaporation fields. The zonal-mean profiles summarize the main aspects of the behavior of evaporation over the oceans. They reveal that the hemispheric evaporation rates tend to be higher during winter than during summer mainly due to the stronger surface winds in winter.

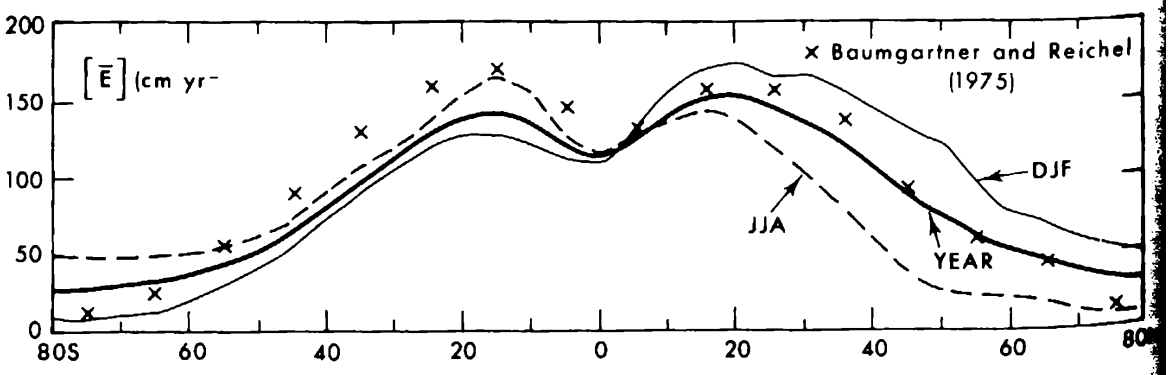

FIGURE 7.27. Meridional profiles of the zonal-mean evaporation rate (in cm yr^{-1}) over the oceans computed using Eq. (10.38) and our 1963–73 surface data. Baumgartner and Reichel's (1975) ocean values from Fig. 7.26 have been added for comparison.

7.6.3 Surface runoff

After considering the precipitation and evaporation fields separately it is useful to compare the behavior of these two quantities since they are closely related elements of climate and hydrology. Thus, we present in Table 7.1 the zonal-mean annual averages of precipitation and evaporation for 10° latitude belts as well as the hemispheric and global averages according to Baumgartner and Reichel (1975). Similar estimates of the same quantities for individual continents and oceans are presented in Table 7.2. The tables include also the $P - E$ differences, the so-called discharge or runoff, and the values of the evaporation ratio E/P and the runoff ratio $(P - E)/P$. These last two quantities are of interest since they are sometimes used as climatic indices or in hydrology studies. Table 7.2 further includes the estimated river discharge R_0 from the continents as measured by the peripheral runoff that reaches the oceans.

The $P - E$ values in Table 7.1 show an excess of precipitation over evaporation at mid and high latitudes as well as in the equatorial zone between 10 °S and 10 °N,

TABLE • 7.1. Estimated mean annual values of the precipitation rate P, evaporation rate E, runoff rate $(P - E)$, evaporation ratio E/P (an aridity index), and runoff ratio $(P - E)/P$ for 10° latitude belts, the hemispheres, and the globe from Baumgartner and Reichel (1975). For comparison, Sellers' (1965) estimates for P and E, and Peixoto and Oort's (1983) independent estimates of $P - E$ as computed from Table 12.1 are shown in parentheses.

	Surface area	*P*	*E*	*P − E*	*E/P*	*(P − E)/P*
80–90 °N	3.9	46 (120)	36 (42)	10 (93)	0.78	0.22
70–80 °N	11.6	200 (185)	126 (145)	74 (124)	0.63	0.37
60–70 °N	18.9	507 (415)	276 (333)	231 (224)	0.54	0.46
50–60 °N	25.6	843 (789)	447 (469)	396 (250)	0.53	0.47
40–50 °N	31.5	874 (907)	640 (641)	234 (156)	0.73	0.27
30–40 °N	36.4	761 (872)	971 (1002)	− 210 (23)	1.28	− 0.28
20–30 °N	40.2	675 (790)	1110 (1246)	− 435 (− 435)	1.64	− 0.64
10–20 °N	42.8	1117 (1151)	1284 (1389)	− 167 (− 322)	1.15	− 0.15
0–10 °N	44.1	1885 (1934)	1250 (1235)	635 (478)	0.66	0.34
0–10 °S	44.1	1435 (1445)	1371 (1304)	64 (144)	0.96	0.04
10–20 °S	42.8	1109 (1132)	1507 (1541)	− 398 (− 342)	1.36	− 0.36
20–30 °S	40.2	777 (857)	1305 (1416)	− 528 (− 312)	1.68	− 0.68
30–40 °S	36.4	875 (932)	1181 (1256)	− 306 (128)	1.35	− 0.35
40–50 °S	31.5	1128 (1226)	862 (895)	266 (150)	0.76	0.24
50–60 °S	25.6	1003 (1046)	553 (520)	450 (278)	0.55	0.45
60–70 °S	18.9	549 (418)	229 (174)	320 (245)	0.42	0.58
70–80 °S	11.6	230 (82)	54 (45)	176 (98)	0.23	0.77
80–90 °S	3.9	73 (30)	12 (0)	61 (32)	0.16	0.84
0–90 °N	255.0	970 (1009)	897 (944)	73 (39)	0.92	0.07
0–90 °S	255.0	975 (1000)	1048 (1064)	− 73 (− 39)	1.07	− 0.07
Globe	510.0	973 (1004)	973 (1004)		1.00	
Units	10^6 km^2	mm yr^{-1}	mm yr^{-1}	mm yr^{-1}		

TABLE • 7.2. Estimated mean annual values of the precipitation rate P, evaporation rate E, runoff rate $P - E$, river runoff rate R_0 from continents into the oceans, evaporation ratio E/P, and runoff ratio $(P - E)/P$ for the various continents and oceans from Baumgartner and Reichel (1975). For comparison, estimates of P, E, and $P - E$ from Sellers (1965) have been added in parentheses.

Region	*Surface area* (10^6 km^2)	P (mm yr^{-1})	E (mm yr^{-1})	P-E (mm yr^{-1})	R_0 (mm yr^{-1})	E/P	$(P - E)/P$
Europe	10.0	657 (600)	375 (360)	282 (240)		0.57	0.43
Asia	44.1	696 (610)	420 (390)	276 (220)		0.60	0.40
Africa	29.8	696 (670)	582 (510)	114 (160)		0.84	0.16
Australia [without islands]	8.9 7.6]	803 [447 (470)]	534 [420 (410)]	269 [27 (60)]		0.67 [0.94]	0.33 [0.06]
North America	24.1	645 (670)	403 (400)	242 (270)		0.62	0.38
South America	17.9	1564 (1350)	946 (860)	618 (490)		0.60	0.40
Antarctica	14.1	169 (30)	28 (0)	141 (30)		0.17	0.83
All land areas	148.9	746 (720)	480 (410)	266 (310)		0.64	0.36
Arctic Ocean	8.5	97 (240)	53 (120)	44 (120)	307	0.55	0.45
Atlantic Ocean	98.0	761 (780)	1133 (1040)	− 372 (− 260)	197	1.49	− 0.49
Indian Ocean	77.7	1043 (1010)	1294 (1380)	− 251 (− 370)	72	1.24	− 0.24
Pacific Ocean	176.9	1292 (1210)	1202 (1140)	90 (70)	69	0.93	0.07
All oceans	361.1	1066 (1120)	1176 (1250)	− 110 (130)	110	1.10	− 0.10
Globe	510.0	973 (1004)	973 (1004)	0 (0)		1.10	0

whereas a deficit of precipitation is found in the subtropics of each hemisphere between about 10° and 40° latitude. In the long-term mean, the excess or deficit in each belt has to be compensated by a net meridional divergence or convergence of water in the particular belt. The runoff ratio $(P - E)/P$ gives an idea of the fraction of the precipitation that is involved in the runoff. The values of the evaporation ratio E/P show clearly the high aridity of the subtropics with ratios larger than 1.

We should stress that there is not always a close agreement between the values of P and E published by different authors, as demonstrated by the comparisons in Tables 7.1 and 7.2 with Sellers (1965) values based on similar observations. Usually the individual values of P and E are adjusted subjectively in a rather arbitrary way by assuming certain global and zonal constraints to yield an overall balance between P and E. This procedure imposes serious limitations on the usefulness of the estimates. The differences are even larger when we compare the results from two different methods, such as in the case of $P - E$ where the independent, aerological estimates are given in parentheses (see column 5, Table 7.1).

Over the globe as a whole, evaporation must balance precipitation in the long-term mean. The precipitation in the two hemispheres is almost the same whereas a large difference is found for the evaporation (about 150 mm yr^{-1}). The higher values of evaporation in the Southern Hemisphere result because this hemisphere is largely covered by oceans. The Northern Hemisphere shows a positive water balance ($P - E = 73$ mm yr^{-1}) whereas in the Southern Hemisphere a net negative value of -73 mm yr^{-1} is found. Thus, we are led to the conclusion that a flow of water in the liquid form must take place across the equator from the Northern into the South-

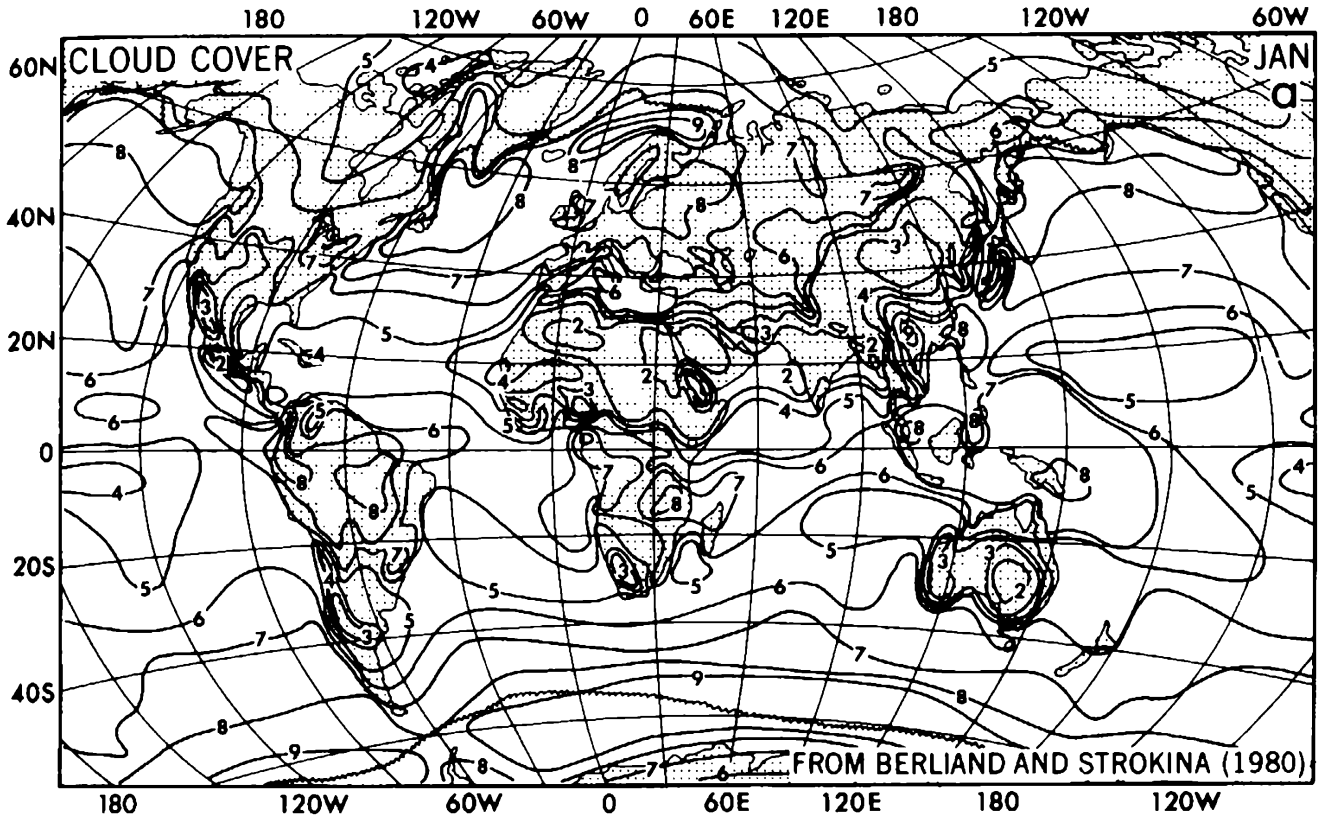

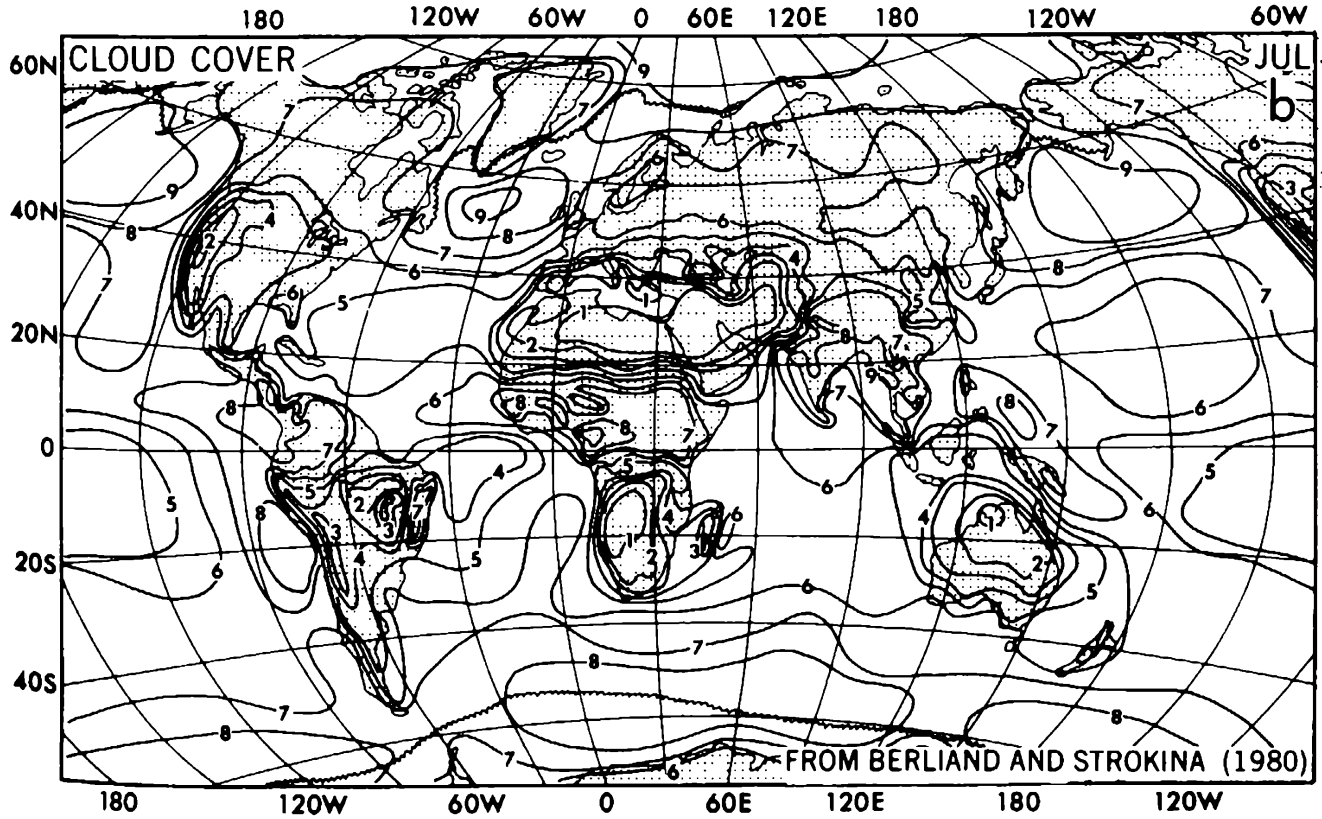

FIGURE 7.28. Global distributions of the cloud cover (in tenths) for January (a) and July (b) after Berlyand and Strokina (1980).

ern Hemisphere. As we will see later, an equal amount of water in the vapor form has to be exported in the opposite direction to maintain the balance of the water substance.

As seen from Table 7.2, the quantities P, E, and $P - E$ are not the same for the different oceans and continents. This is not only due to physiographic differences between them but also due to the differences in areal extent. For example, South America shows the highest P, E, and $P - E$ values in agreement with what we have seen before on the corresponding global maps. On the other hand, Australia, Africa, and Antarctica show very small runoff ($P - E$) values. Overall, the precipitation and evaporation tend to be smaller over the continents than over the oceans, except for the extremely high values of P and E over South America and the extremely low values of P and E over the Arctic Ocean. The mean value of $P - E$ over all continents is estimated to be 266 mm yr^{-1} This surplus of condensed water must be transported by rivers and glaciers from the continents into the oceans where a deficit of -110 mm yr^{-1} is found. When the surplus over land and the deficit over the oceans are multiplied by the appropriate areal factors they must balance. The table further shows that $P - E$ is positive for the Arctic and Pacific Oceans and strongly negative for the Atlantic and Indian Oceans (the "dry" oceans) leading to the net deficit for all oceans combined. The implications of these estimates of $P - E$ taken together with the values of the observed river discharge are that a net transfer of water must occur from the Pacific and Arctic Oceans into the Atlantic and Indian Oceans. For example, water transport by the rivers from the surrounding continents into the Atlantic is estimated to be on the order of $R_0 = 197$ mm yr^{-1} so that the equivalent of $E - P - R_0 = 175$ mm yr^{-1} must come from the Pacific and Arctic Oceans. Further, for the Indian Ocean which only receives 72 mm yr^{-1} from continental runoff an inflow of 179 mm yr^{-1} must take place from the Pacific Ocean. The net excess of precipitation over evaporation over the continents must be maintained by a net influx of water in vapor form from the large ocean sources.

The crude picture of the global water transfers in the climate system sketched so far will be further extended in Chap. 12.

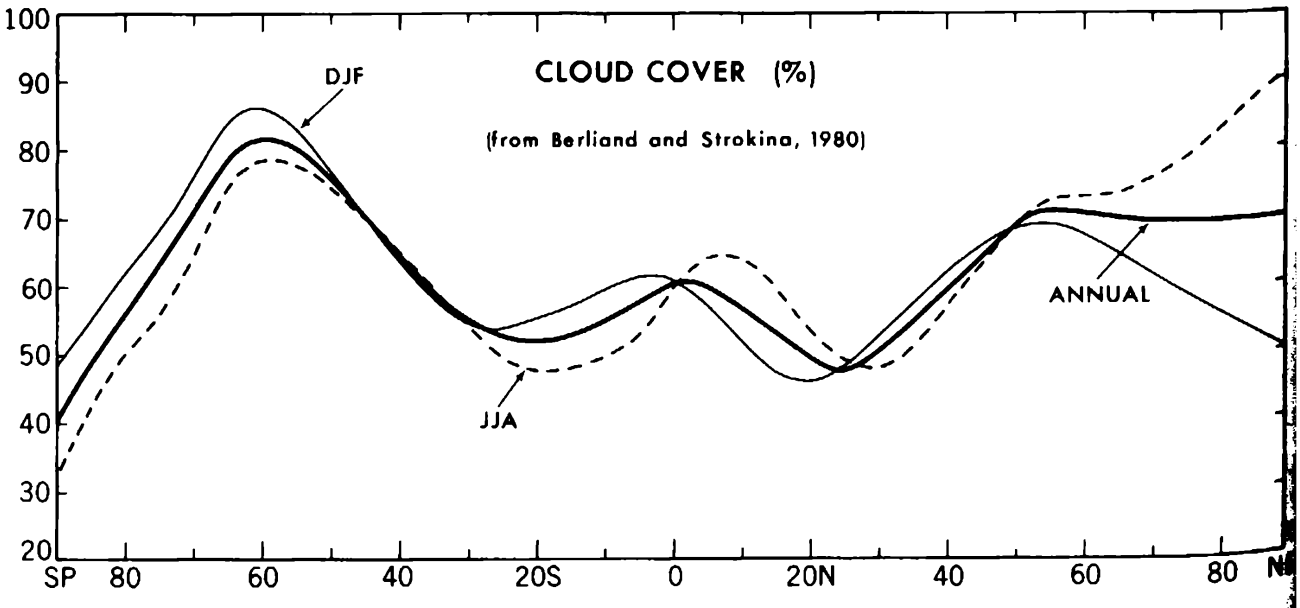

FIGURE 7.29. Meridional profiles of the zonal-mean cloud cover (in %) for annual, DJF, and JJA mean conditions based on data from Berlyand and Strokina (1980).